In Situ Monitoring of an *Escherichia coli* Fermentation Using a Diamond Composition ATR Probe and Mid-infrared Spectroscopy

Denise L. Doak and Janice A. Phillips*

Department of Chemical Engineering, Lehigh University, Bethlehem, Pennsylvania 18015

A diamond composition ATR probe was used in situ to obtain IR spectra on replicate *Escherichia coli* fermentations involving a complex medium. The probe showed excellent stability over a 6-month operating period and was unaffected by either agitation or aeration. The formation of an unknown was observed from IR spectra obtained during the sterilization; subsequent experiments proved this to be a reaction product between yeast extract and the phosphates used as buffer salts. Partial-least-squares-based calibration/prediction models were developed for both glucose and acetate using in-process samples. The resulting models had prediction errors of ±0.26 and ±0.75 g/L for glucose and acetic acid, respectively, errors which were statistically equivalent to the estimated experimental errors in the reference measurements. Relative concentration profiles for the unknown formed during sterilization could be generated either by tracking peak height at an independent wavelength or by self-modeling curve resolution of the spectral region overlapping that of glucose. These profiles indicated that this compound was metabolized simultaneously with glucose; upon depletion of the glucose, when the microorganism switched to consumption of acetic acid, utilization continued but at a lower rate. The data presented provide an extensive characterization of the performance characteristics of this in situ analysis and clearly demonstrate its utility not just in the quantitative measurement of multiple known species but in the qualitative evaluation of unknown species.

Introduction

Over the past decade, there has been an increasing interest in using both near-infrared (Brimmer and Hall, 1993; Cavinato et al., 1990; Chung and Arnold, 1995; Chung et al., 1995, 1996; Hall et al., 1996; He et al., 1993; Kasprow et al., 1998; Macaloney et al., 1994, 1995; Nishinari et al., 1989; Silman et al., 1983; Vaccari et al., 1994) and mid-infrared (Alberti et al., 1985; Bellon-Mauriel et al., 1995; Fairbrother et al., 1989; Fayolle et al., 1996; Hopkinson et al., 1987; Hutson et al., 1988; Kuehl and Crocombe, 1984; Sowa and Towill, 1990; Tseng et al., 1996; White et al., 1985; Wong et al., 1984) spectroscopy to monitor biological processes. While a number of diverse process systems have been investigated, most of the results reported to date have been on the off-line application of this technology. Only a limited amount of work has been done with on-line monitoring (Fairbrother et al., 1991; Hammond and Brookes, 1992), and no demonstration of the usefulness of the technology in closed loop control has been completed. In those few cases in which on-line monitoring has been explored, sampling from the bioreactor has been implemented with a recirculating loop configuration, the practicality and long-term ruggedness of which is somewhat problematic.

The relative qualitative and quantitative merits of both near- and mid-infrared spectroscopy have been considered for a variety of systems (Cooper et al., 1997; Doyle, 1995; Lee et al., 1993; Stallard, 1997; Yu and Phillips, 1992). Mid-infrared spectroscopy measures the fundamental vibrational modes of molecules (Colthup et al., 1990; Peters et al., 1974; Robinson, 1995; Smith, 1979). As a consequence, it has a unique advantage over near-infrared spectroscopy: not only can known species be quantified, but unknown species that frequently arise in complex systems can be detected and identified. Used in situ, the mid-infrared spectrometer has proven to be extremely valuable in detecting transient chemical species that cannot be captured for off-line analysis. The method is unconstrained by dynamic range and, within the performance limits of the instrument components, has excellent sensitivity. The sampling systems available for liquid phase analysis are all based on attenuated total reflection (Harrick, 1979). This concept has been readily adapted to probe configurations which facilitate interfacing the spectrometer to the process (Doyle and Jennings, 1990; Landau and Rein, 1993; Milosevic et al., 1995). The materials of construction of these probes allow for use under extremely harsh conditions. The major limitation in applying such probe technology to bioreactors has been in custom designing the probe to fit the unique port design typical of most fermentors.

In this paper, we report results on the in situ monitoring of both the sterilization and batch operation cycles of a bench-scale fermentor obtained using a diamond composition ATR probe specifically designed to fit a 25 mm Ingold port. The model fermentation system selected for these studies was *Escherichia coli*.

Materials and Methods

Microorganism, Medium, and Inoculum Preparation. *E. coli* strain AR 58 (F- thr- galE::Tn10 rpsL cI857 ΔH1), a defective λ lysogen of the *E. coli* strain N99, was

* To whom correspondence should be addressed.

10.1021/bp990039b CCC: $18.00
Published on Web 04/24/1999

obtained from SmithKline Beecham (King of Prussia, PA). Stock cultures of the microorganism were maintained frozen in 1.8 mL cryotubes in 15% glycerol at −70 °C. To initiate a fermentation, two cryotubes were thawed at room temperature and added to each of two 250 mL baffled shake flasks containing 50 mL of Luria broth (containing 10 g/L bacteriological grade tryptone, 5 g/L bacteriological grade yeast extract, 5 g/L NaCl). The flasks were incubated on a New Brunswick Scientific G25 gyratory air incubator for 9 h at 30 °C and 200 rpm. After microscopic examination, the flasks were pooled and 5 mL added to each of 10 500 mL baffled shake flasks containing 100 mL of a medium consisting of 25 g/L glucose, 0.865 g/L KH_2PO_4, 7.65 g/L K_2HPO_4, 12 g/L bacteriological grade tryptone, and 24 g/L bacteriological grade yeast extract. These flasks, which were used to inoculate the fermentor, were incubated at 30 °C for 12 h on the incubator shaker. The medium used in the fermentor was identical to that used in the inoculum shake flasks.

Fermentor and Fermentation Operating Conditions. The data reported in this paper are from three replicate fermentations—referred to as EC001, EC002a, and EC003. All fermentations were conducted in a Biostat E fermentor (B. Braun Biotech, Inc., Allentown, PA). The unit is fully integrated with microprocessor based modules for monitoring and/or controlling pH, dissolved oxygen, temperature, and foam level. The unit was equipped with an in-place sterilizable ES stainless steel vessel with a total volume of 15 L and a recommended working volume of 10 L. The vessel was outfitted with three turbine impellers.

To prepare the fermentor, the vessel was filled with 8 L of distilled, deionized water. The medium components listed above, with the exception of the glucose, were added individually, in sequence from the least to the most concentrated. Ten milliliters of PEG 1200 was also added as an antifoam agent. The vessel was sterilized with a hold time at 121 °C of 30 min. Prior to inoculation, 1 L of a 250 g/L sterile glucose solution was added aseptically. Fermentations were conducted at 30 °C, with pH controlled at 7.0 by the addition of either 5 N H_2SO_4 or NaOH and dissolved oxygen controlled at ≥20% saturation at atmospheric conditions by varying the agitation speed from 200 to 800 rpm.

Spectrometer, Probe, and Spectral Acquisition Parameters. The ReactIR 1000 (ASI Applied Systems, Millersville, MD) was used for the acquisition of mid-IR spectra. This system consists of an electronics module, optical module, chemistry sampling system, and computer workstation. The sampling system used for these experiments was a DiComp multireflection diamond ATR insertion probe specifically modified to insert through a 25 mm Ingold-like port on the Braun ES vessel. This probe, which is $^5/_8$ in. in diameter and 7.25 in. long and is constructed of stainless steel, has a six-reflection diamond/ZnSe bilayer ATR element, 3 mm in diameter, at its tip. The IR absorption characteristics of the diamond layer restrict the wavenumber range for the probe to 4000−2200 and 1900−700 cm^{-1}. The probe was interfaced with the optical module of the ReactIR 1000 via an optical conduit, as depicted in Figure 1; of the four joints in this conduit, at each of which are mirrors to collimate the IR beam, only one could be adjusted during instrument alignment. The system was equipped with an MCT detector in a 12-h liquid N_2 dewar. The probe and optical path were purged continuously with gas at 2500 cm^3/h, 10 psig provided by a Balston Model 75-45 FT-IR purge gas generator equipped with a Balston

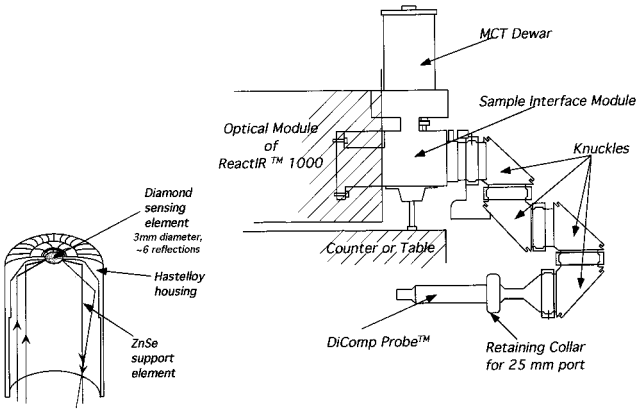

Figure 1. Schematic of ReactIR1000 interfaced with DiComp probe designed for a 25 mm fermentor port.

Model 72-428 single flow controller (Whatman, Inc., Haverhill, MA). The workstation was provided with ReactIR vers.1.3 or vers. 2.0 software that was used to operate the spectrometer, analyze the spectra, and develop calibration/prediction models.

Unless otherwise noted, all single beams were comprised of 512 coadded scans taken at 4 cm^{-1} resolution over the range of 4000−500 cm^{-1} with Happ−Genzel apodization and autogain ranging. During batching of the fermentor, single beams were acquired on the empty dry vessel, after distilled water addition and after the addition and dissolution of the individual medium components. Once water was added to the vessel, the contents were thermostated at 30 °C and agitated at 200 rpm. During sterilization monitoring, single beams were obtained every 10 min for 180 min; during fermentation monitoring, single beams were obtained every 10 min for 15−24 h.

Off-Line Analyses. Samples were withdrawn from the fermentor at intervals of 10−60 min. The optical density of the whole broth was measured at 650 nm in a 1 cm path length polystyrene disposable cuvette using a Bausch & Lomb Spectronic 601 UV/vis spectrometer; the sample was appropriately diluted to maintain the absorbance reading between 0 and 0.6. A 5 mL aliquot of the whole broth was centrifuged at 3000 rpm in an IEC clinical centrifuge. The supernatant from the centrifugation and the residual whole broth sample were frozen at −32 °C pending additional off-line analyses.

Glucose concentrations of the supernatants were measured with the YSI Model 2700 SELECT biochemistry analyzer (YSI Inc., Yellow Springs, OH).

Acetic acid concentrations were determined by HPLC using a Bio-Rad HPX-87H column, thermostated at 35 °C and equipped with a precolumn; the eluant, 0.01 N H_2SO_4, was pumped at 0.6 mL/min.

Results and Discussion

Performance Characteristics of ReactIR 1000 and DiComp Probe. A variety of tests were conducted to assess the stability of the ReactIR 1000 spectrometer and DiComp probe and define its performance characteristics.

The short-term stability of the system was evaluated by collecting single beams, each consisting of 512 coadded scans, once an hour over a 40-h period; during this test the fermentor contained water thermostated at 30 °C and agitated at 200 rpm. The average of the 41 single beams collected, along with the standard deviation as a function of wavenumber, is presented in Figure 2a. As

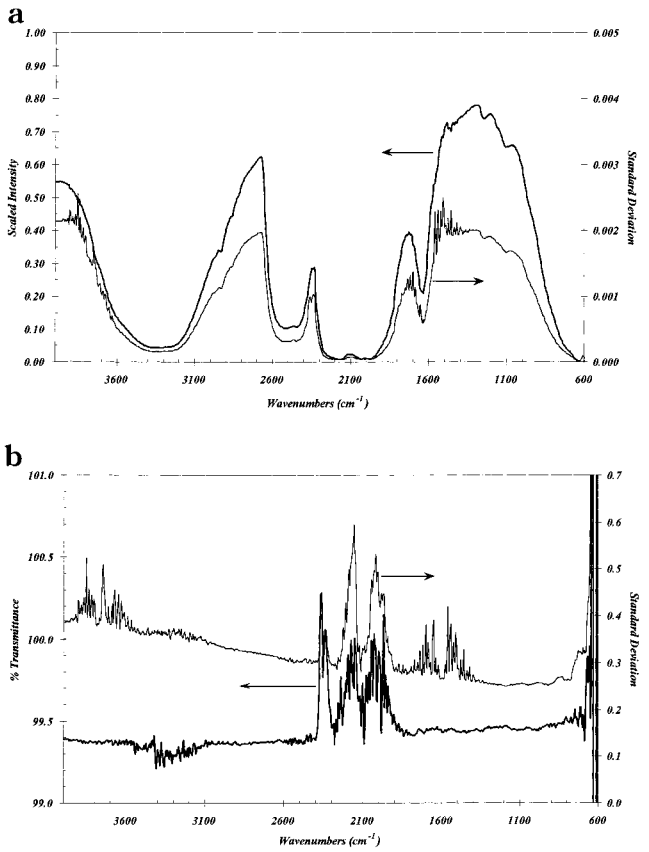

Figure 2. Short-term stability of the ReactIR1000/DiComp probe: (a) average and standard deviation of single beams collected hourly over a 41-h period; (b) average 100% line and standard deviation calculated with a H_2O single beam as the background.

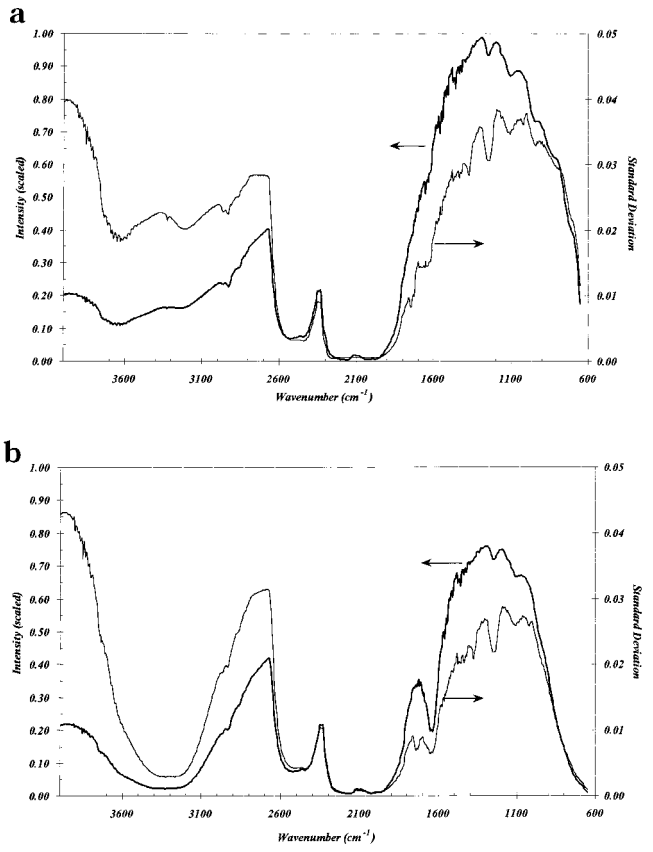

Figure 3. Long-term stability of the ReactIR1000/DiComp probe: (a) average and standard deviation of air single beams collected over approximately 6 months; (b) average and standard deviation of water single beams collected over the same operating period.

expected, the variation in the single beam intensity is a function of wavenumber. The largest absolute variations occur over those wavenumber ranges for which the signal is large; the relative variations, however, are small, averaging ±0.41% (4000−3600 cm^{-1}), ±0.37% (3600−3100 cm^{-1}), ±0.33% (3100−2600 cm^{-1}), ±0.32% (2600−2200 cm^{-1}), ±0.27% (1900−1600 cm^{-1}), ±0.41% (1600−1000 cm^{-1}), and ±0.29% (1000−650 cm^{-1}). The impact of this level of variability is more easily seen in the 100% transmittance line shown in Figure 2b; the data for this figure were calculated by normalizing the single beams to a water single beam collected as background prior to the start of the test. Again, the variation in the 100% T line is a function of wavenumber. The regions of highest variation—between 2200 and 1900 cm^{-1} and below 650 cm^{-1}—correspond to those frequencies at which the diamond absorbs most or all of the energy. Outside this region, the variations in the 100% T line are identical to those reported above for the single beams.

The longer-term stability of the system, which has practical implications for the implementation of calibration/prediction models, is illustrated by single beams collected over an approximate 6-month period. The averages of the single beams (each consisting of 512 scans) and their standard deviations are shown in parts a and b of Figure 3 for air and water, respectively. The data are presented for both, as either is an appropriate reference for calculation of the absorbance spectrum of a sample. Again, there is some variability at all wavenumbers except over the 2200−1900 cm^{-1} range, where the diamond absorbs most or all of the energy. As might be anticipated, over this longer time frame, the magnitude of both the absolute and relative variability is greater. In both cases, above the upper wavenumber cutoff of the diamond (i.e., 2200 cm^{-1}), the relative variability ranges between 4 and 20%, increasing with increasing wavenumber. Below the lower wavenumber cutoff of the crystal (i.e., 1900 cm^{-1}), the relative variability is 2−4% over the range from 1200 to 1900 cm^{-1} and gradually increases to ∼7% below 1200 cm^{-1}. The longer-term variability in system performance is higher than that measured over 40 h for obvious reasons. Over the 6 months of operation, the fermentor and spectrometer were shut down and disassembled several times for maintenance of and mechanical repairs to the fermentor. Thus, the longer term stability analysis is representative of significantly different experimental and system factors.

A more conventional measure of system performance is the signal-to-noise (SNR) ratio (Griffiths and de Haseth, 1986; Smith, 1996; Strobel and Heineman, 1989). In Table 1 are summarized the SNRs measured at random time intervals over a 9-month period; five measurements, each comprised of a sample and background measured on air at 160 scans, were taken at each time and the SNRs calculated for the wavenumber range 1200−1100 cm^{-1} from the root-mean-square (rms) noise estimate over this region. The overall average SNR of 12 989 ± 1495 is equivalent to a rms noise of 0.000 078 ± 0.000 005 AU (absorbance units). Thus, for this instrument, these data indicate that the limit of detection is 0.000 234 AU (Strobel and Heineman, 1989) over the range 1200−1100 cm^{-1}.

A more accurate picture of the noise structure across the spectral range between 1900 and 650 cm^{-1} is given in Figure 4. In this case, the rms noise level was calculated at each wavenumber using five absorbance

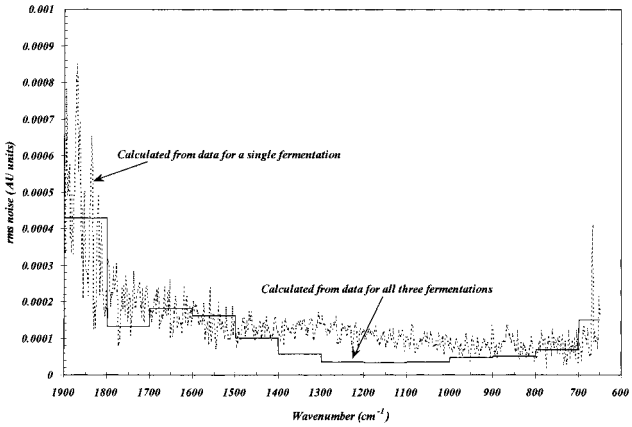

Figure 4. Rms noise as a function of wavenumber.

Table 1. Signal-to-Noise Characteristics of ReactIR and DiComp Probe

elapsed operating time (days)	signal-to-noise ratio					average	std dev
0	11886	14544	13276	11828	14795	13266	1409
10	13870	12289	14454	15896	12714	13845	1439
38	9647	13818	15754	12306	13921	13089	2280
43	11555	12716	11823	11616	12692	12080	578
44	15411	10904	11720	13888	12127	12810	1817
48	9795	10328	12481	13899	11179	11537	1665
57	14047	12937	13960	13255	13597	13559	469
66	15308	13612	8907	13613	13531	12995	2404
73	14961	12330	14722	14225	14949	14237	1107
84	11556	11965	10419	13963	11727	11926	1284
106	14016	14413	11479	11435	13307	12930	1402
108	15604	13067	12301	12915	13697	13517	1268
116	12506	13754	14377	12085	15919	13728	1534
119	11515	12736	15816	12561	11249	12775	1817
134	12422	13414	12093	14604	16472	13801	1785
136	9505	12457	10358	10160	13905	11277	1839
143	11237	11372	11842	12881	11494	11765	663
169	15430	16503	12364	11802	10931	13406	2422
173	12237	12410	13046	14084	14951	13346	1153
212	12080	14088	15080	14486	12382	13623	1323
220	14565	10448	12402	15960	14936	13662	2215
231	16238	12612	13598	12315	12023	13357	1716
280	13323	12374	12373	11317	11487	12175	807
281	11960	11985	13360	15474	12381	13032	1478

overall average SNR	12989
std dev	1495
average rms noise	0.000078
std dev	0.000005

spectra collected prior to one of the fermentations (Mark and Workman, 1991). Superimposed over these data is the rms noise level calculated over 100 cm^{-1} intervals using 15 absorbance spectra collected for all three fermentations. As is clear from this figure, the rms noise varies significantly across the spectral range. Over the range of interest for monitoring most species important in biological systems (i.e., 1900−650 cm^{-1}), the rms noise varies from a maximum (averaging 0.000 41 ± 0.000 19 AU) between 1900 and 1800 cm^{-1} to a minimum (averaging 0.000 11 ± 0.000 03 AU) between 1500 and 900 cm^{-1}. Consequently, it can be expected that the limit of detection for any chemical species will be highly dependent on the wavenumber range over which it absorbs. Practically, the limit of detection is determined not just by the inherent SNR of the instrument; manipulation of the spectral data (e.g., through second-derivative analysis), calibration methodology, and intrinsic error of the calibration data used can all influence the observed sensitivity.

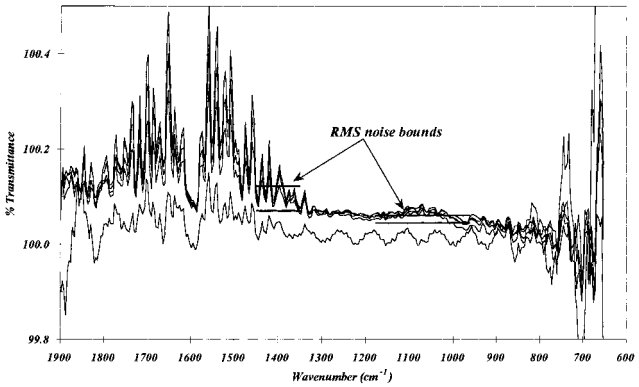

Figure 5. Effect of agitation speed on the 100% transmittance line.

Several tests were conducted to determine the effect of reactor operating conditions on the spectrometer performance. In the first, to determine the effect of agitation speed, single beams were collected every 5 min for a period of 30 min at 100, 300, 500, 700, and 900 rpm. At each speed, the seven single beams collected were ratioed to a water single beam collected at 200 rpm and averaged. The 100% transmittance lines at each speed are plotted in Figure 5 between 1900 and 650 cm^{-1}. For comparison, ±1 rms noise level (calculated for these specific data in % T) is shown for 1450−1350 and 1180−960 cm^{-1}, the wavenumber ranges used in the calibration/prediction models for acetic acid and glucose, respectively. Within the bounds defined by the standard deviations of the measurements and by the rms noise, there appears to be little or no effect of agitation speed on the system performance. The spectral activity between 1850 and 1350 cm^{-1} corresponds to ranges for the −C═O stretch and may be indicative of the dissolution of CO_2 (and the formation of its associated equilibrium carbonate species) during the test (Colthup et al., 1990; Lin-Vien et al., 1991; Smith, 1979).

The objective of the second test was to determine the effect of aeration on the spectrometer/probe performance. Single beams were acquired once every 10 min for 1 h on the unaerated, thermostated, agitated tank containing water. The spectral acquisition was repeated with the vessel aerated at 1 vvm. The 13 single beams acquired for both cases were averaged, and the average was ratioed to a water single beam to obtain the 100% transmittance lines shown in Figure 6. Again, there was no observable, significant effect of aeration on the instrument performance.

To evaluate the impact of temperature variations on the infrared spectra, single beams on water were acquired once every 10 min on the vessel containing water only while it was run through a typical sterilization cycle; temperatures at the beginning and end of each spectral acquisition were recorded. The results from this study are shown in Figure 7. For reference, the spectrum of water at 30 °C (calculated with an air single beam as background) is also shown in this figure; this spectrum has two major peaks: one centered around 3300 cm^{-1} characteristic of the −OH stretch, the other centered around 1650 cm^{-1} characteristic of the −OH bend. It is obvious from the data presented in Figure 7 that temperature has two distinct effects on the IR absorption characteristics of water. First, changes in temperature affect the intensities of both the stretching and bending frequencies of the water molecule, as indicated by the changes in the height of the two characteristic peaks of water. In addition, in regions outside these characteristic

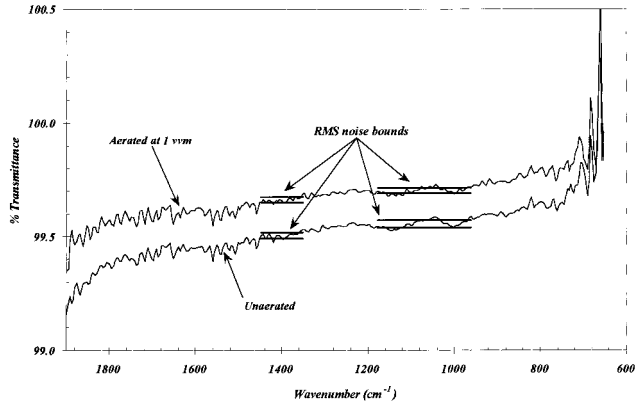

Figure 6. Effect of aeration on the 100% transmittance line.

absorption frequencies, there is a shift upward in the spectral baseline. Some of these effects may be due to changes in the refractive index of the surrounding medium (the refractive index of diamond is independent of temperature over the range explored). However, theoretical calculations indicate that the depth of penetration (d_p, i.e., the optical path length) decreases with increasing temperature and that percentage change in d_p is independent of wavenumber. In those cases for which temperature is a variable, it may be possible to incorporate both of these effects as factors in the calibration/prediction model, mitigating their impact on the robustness of the concentration estimates (Hazen et al., 1994).

IR Absorption Characteristics of Medium Components. The IR absorption characteristics of the individual medium components were calculated from the single beams obtained during batch preparation of the vessel. The resulting absorbance spectra, obtained by ratioing the appropriate sequential single beams, are shown in Figure 8a−f for KH_2PO_4, K_2HPO_4, tryptone, yeast extract, PEG 1200, and glucose, respectively. The spectra of well-defined components, such as KH_2PO_4, K_2HPO_4, and glucose, are characterized by relatively sharp absorbance features. For example, as shown in Figures 8a,b, the spectra of both KH_2PO_4 and K_2HPO_4 exhibit an absorbance feature between 1100 and 1000 cm^{-1} characteristic of the PO_4^{3-} group and an absorbance feature between 1000 and 900 cm^{-1} characteristic of the P−OH bond. KH_2PO_4 can be distinguished, however, on the basis of the additional absorbance feature that appears between 1200 and 1100 cm^{-1} as a consequence of the additional −OH group. Complex medium components, such as tryptone and yeast extract, exhibit more complicated absorption patterns. Both, however, absorb IR radiation with the regions characteristic of carbon and nitrogen containing organic materials. PEG 1200, used as an antifoam, exhibits a single, broad absorption feature around 1100 cm^{-1}. With the exception of the anomalous behavior of the spectrum for KH_2PO_4 for fermentation EC001, all spectra were highly reproducible.

Effect of Sterilization on Medium Components. The IR spectra obtained during monitoring of the sterilization are shown in Figure 9; during acquisition of these spectra, the temperature increased from 30 to 121 °C and decreased back to 30 °C. As previously noted, some of the changes in these spectra are due to the effect of temperature on the intrinsic IR absorption characteristics of the components, including the water. However, the spectra also clearly illustrate the changes in medium character resulting from sterilization. As shown by the difference spectra in Figure 10, these changes occur over the 1250−850 cm^{-1} wavenumber range with distinct features in the regions characteristic of carbohydrates (1250−950 cm^{-1}) and phosphorylated compounds (1000−900 cm^{-1}) (Lin-Vien, 1991). On the basis of additional experiments that have been conducted in which medium components were sterilized alone and in various combinations, it was determined that these changes are a

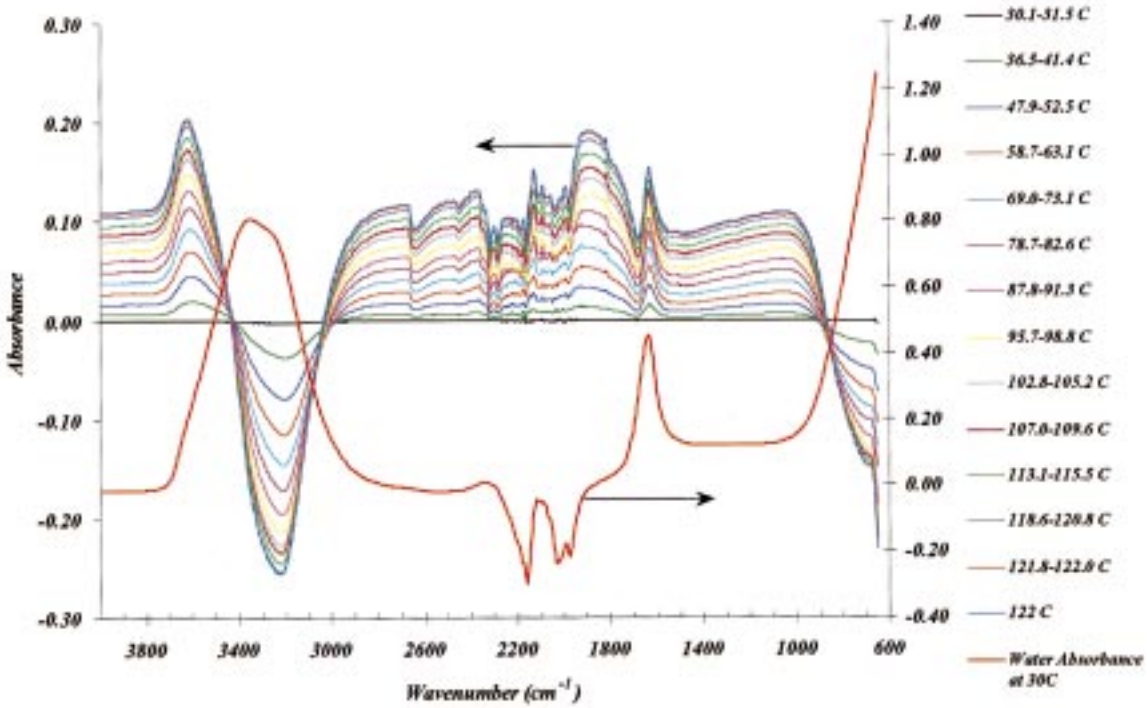

Figure 7. Effect of temperature on the absorbance spectrum of water over the temperature range typical of a sterilization cycle. All absorbance spectra were calculated relative to the single beam of H_2O at 30 °C. Also shown is the absorbance spectrum of H_2O at 30 °C.

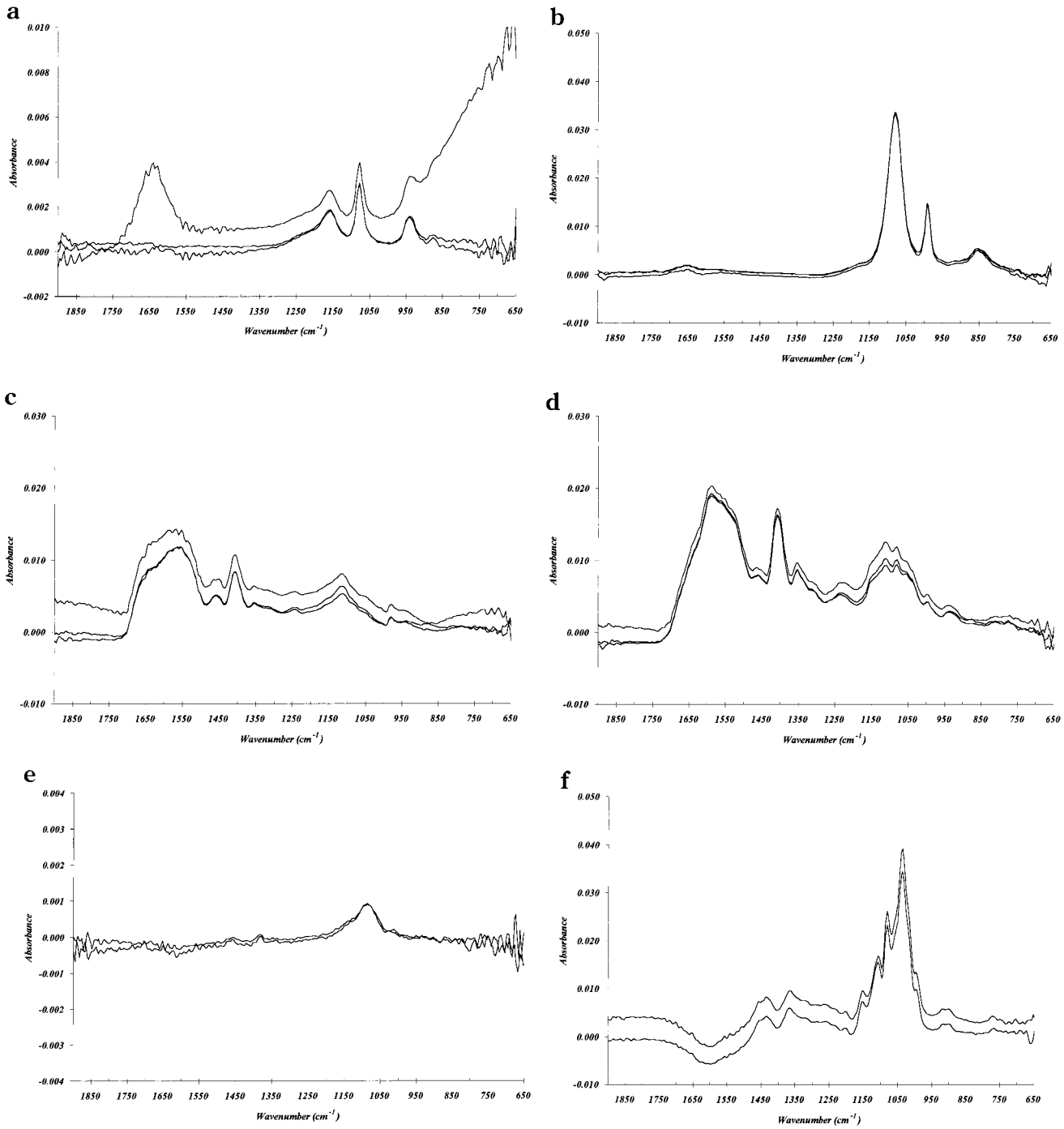

Figure 8. IR absorbance spectra of individual medium components: (a) KH_2PO_4 at 1.08 g/L; (b) K_2HPO_4 at 9.56 g/L; (c) bacteriological grade tryptone at 15 g/L; (d) bacteriological yeast extract at 30 g/L; (e) PEG 1200 at 1.25 mL/L; (f) glucose at 25 g/L. Spectra were calculated by ratioing successive single beams obtained during batching of the fermentor; all single beams were measured at 30 °C. Concentration for phosphates, tryptone, yeast extract, and antifoam are based on 8 L of distilled H_2O.

consequence not of autolysis of the complex medium components but of reactions between the yeast extract and phosphates. The spectra also indicate the differences that can occur among sterilization cycles. Despite the fact that all three sterilizations were conducted in an identical fashion, the quantity of these reactions products formed was significantly higher in EC002a than in EC001 or EC003. This was apparently not a consequence of any differences in the sterilization cycles, all of which were essentially identical in terms of the heat-up, hold, and cool-down times. An alternative explanation is a difference in the phosphates used since the source of these materials (other than to use reagent grade chemicals) was not precisely controlled; however, the pure component spectra calculated from the single beams obtained during batching do not support this explanation. Both the presence and relative magnitude of this compound are important. It has been determined that the reaction product is easily metabolized during the initial phase of the fermentation. Differences in the quantity of this reaction product produced during sterilization may account for subtle differences in the initial fermentation pattern.

Monitoring and Quantification of Metabolites during Fermentation. A typical spectral profile obtained during the course of the fermentation monitoring is presented in Figure 11. For this profile, the single beams were ratioed to water. The decrease in absorbance

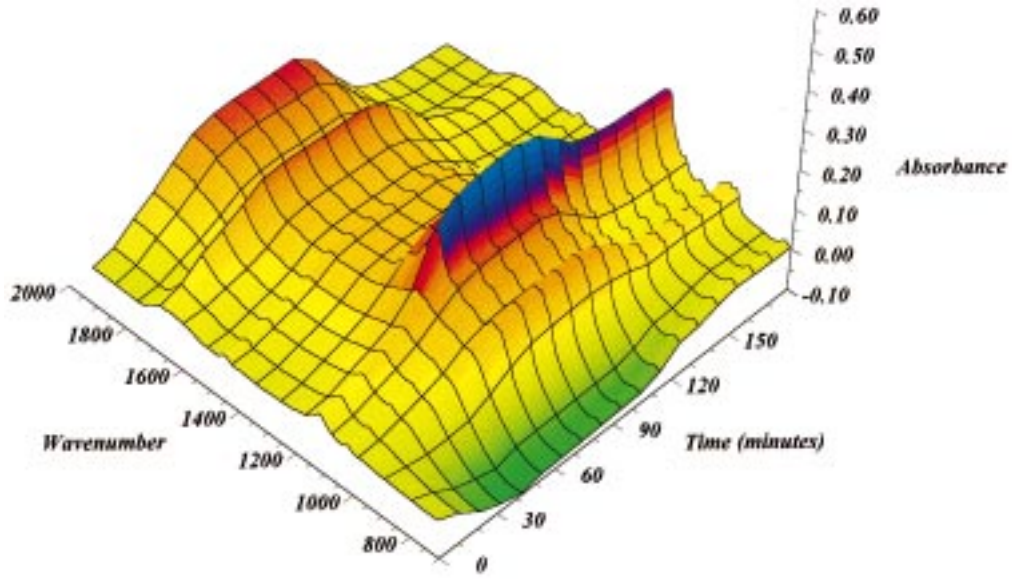

Figure 9. Profile of IR spectra obtained every 10 min during sterilization. Typical times for each segment of the cycle were 1 h for heat-up from 30 to 121 °C, 40 min hold at 121 °C, 24−42 min for cool-down from 121 to 30 °C.

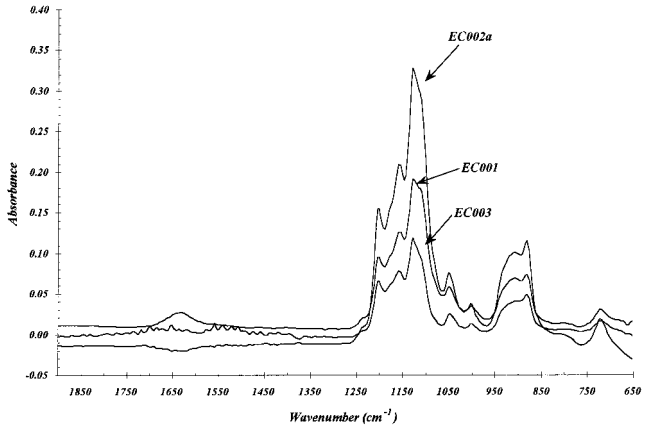

Figure 10. Difference spectra calculated from absorbances measured before and after sterilization of the medium without glucose.

in the 1300−1000 cm^{-1} range results from the consumption of both glucose and the phosphorylated carbohydrate formed during the sterilization. The decrease in the latter can also be observed from the profile of absorbance in the 1000−850 cm^{-1} range. The increase in absorbance over 1700−1400 cm^{-1} is due to the accumulation of organic acids.

The off-line measurements of glucose and acetate from all three fermentations (101 samples total) were used to develop a calibration/prediction model based on the partial least squares (PLS) (Martens and Naes, 1989) routine that is part of the ReactIR software package. Individual models were developed for each species on the basis of their characteristic absorbance wavelengths and validated using leave-one-out cross-validation. In developing the initial models, several factors relating to the multivariate analysis were considered: type of background to be used (air, water, or medium without glucose addition), type of baseline, specific wavelength range, and number of factors. The effect of each of these variables on the root-mean-square error of prediction for glucose is illustrated in Figure 12. In the case of glucose, the choice of background had the most significant effect on the model prediction error: the use of medium without glucose as background essentially buries the spectral features of the phosphorylated carbohydrate, which were changing with time, in the background.

On the basis of this analysis, it was decided, for development of the initial models, to use water as background, a two-point baseline, and 10 factors in the calibration model. For glucose, the wavenumber range used was 1180−960 cm^{-1}; for acetic acid, the wavenumber range was 1450−1350 cm^{-1}. The initial models were subjected to a Studentized *t* deleted residual analysis to detect and eliminate concentration outliers. This analysis reduced the number of data points in the calibration/prediction models to 91 for glucose and to 75 for acetic acid. The difference is reflective of the greater variability observed in the off-line HPLC analysis for acetic acid than that seen in the YSI analysis of glucose. A comparison of the measured and predicted concentrations of glucose and acetic acid for all three fermentations is given in parts a and b of Figure 13, respectively. The leave-one-out cross-validation error was ±0.26 g/L for glucose and ±0.75 g/L for acetic acid. These errors are statistically equivalent to the errors in the off-line measurements (0.20 ± 0.24 for the YSI analyzer; 0.22 ± 0.45 for the HPLC) and are comparable to the lowest errors previously reported for near (Chung et al., 1996; Hall et al., 1996, Hazen et al., 1994; Macaloney et al., 1996; Vaccari et al., 1994) and mid-IR (Bellon-Mauriel, 1995; Fayollle, 1996) analysis of the same species. It should be noted, however, that, in the above studies, different approaches were taken to both spectral manipulation and calibration and, in those cases involving *E. coli*, the medium composition was different.

The relative concentration of the unknown produced during sterilization was determined in two ways: (1) by profiling the absorbance maximum that occurs at ∼880 cm^{-1} and that is a unique feature of this compound and (2) by employing a self-modeling curve resolution algorithm (Hamilton and Gemperline, 1990) between 1225 and 960 cm^{-1}, which overlaps the absorbance range for glucose. The first analysis was conducted using the profiling software available in ReactIR vers. 2.0; the second analysis was conducted with the ConcIRT Opus I software available from ASI Applied Systems. In the latter analysis, a fixed glucose spectrum was defined. A

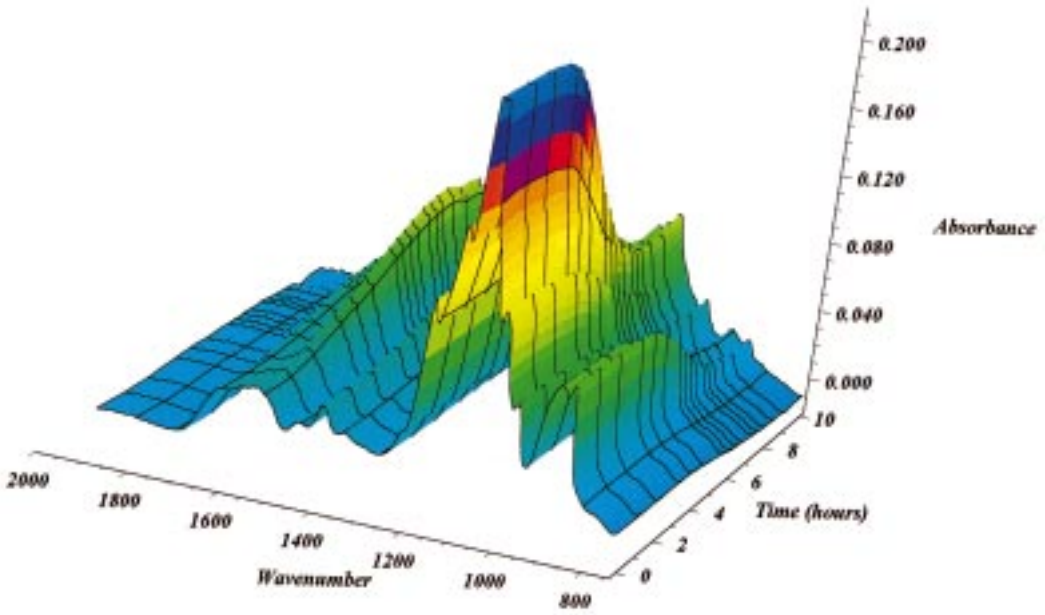

Figure 11. Profile of IR spectra obtained every 10 min during fermentation.

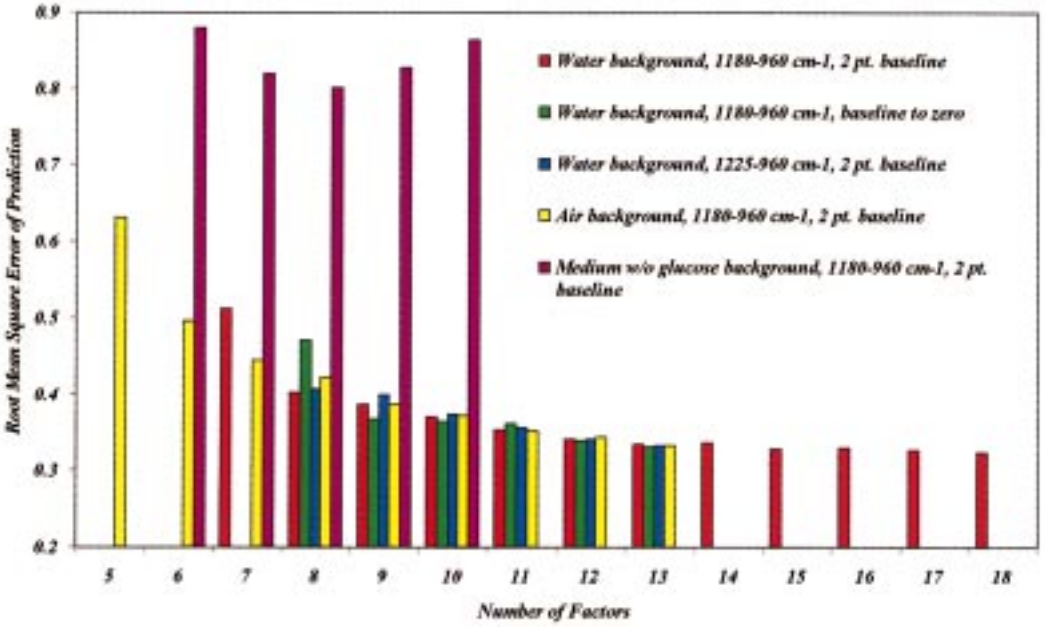

Figure 12. Effect of calibration model parameters on rms error of prediction for glucose.

typical profile of relative concentration on a 0−100% scale obtained by these procedures is given in Figure 14. As shown in Figure 15, this compound is cometabolized with glucose, with a slight lag between the start of its utilization and that of glucose. When glucose is depleted and the microorganism switches to metabolism of the accumulated acetic acid, utilization of the unknown continues but at a significantly slower rate. In two of the three fermentations conducted (i.e., EC001 and EC002a), the unknown was still present at 11 h; in fermentation EC003, the compound was essentially depleted at approximately 9.5 h (unpublished data). This trend is in agreement with that observed in the magnitude of the absorbance measured at $t = 0$ h, as shown by the difference spectra of Figure 11.On the basis of the data obtained, depletion of this compound did not affect acetate utilization. However, higher levels of acetic acid accumulated in those fermentations in which the initial amount of this unknown was also higher.

Conclusions

The data presented are intended to demonstrate the utility of an in situ mid-infrared probe in obtaining both a quantitative and qualitative characterization of the *E. coli* fermentation. The system has been shown to have excellent stability properties, unaffected by agitation or aeration rates or shutdowns imposed by routine maintenance procedures. The current design operates at a SNR that allows the detection of a ±0.000 33 AU (± 3 × rms noise level) over the wavenumber range corresponding to glucose absorbance. Changes in system design, such as increases in the number of reflections, could enhance this SNR and decrease the limit of detection. It has also been shown by the case of the unknown produced during sterilization that was metabolized during fermentation and which may have some role in acetate formation that the methodology possesses the unique ability

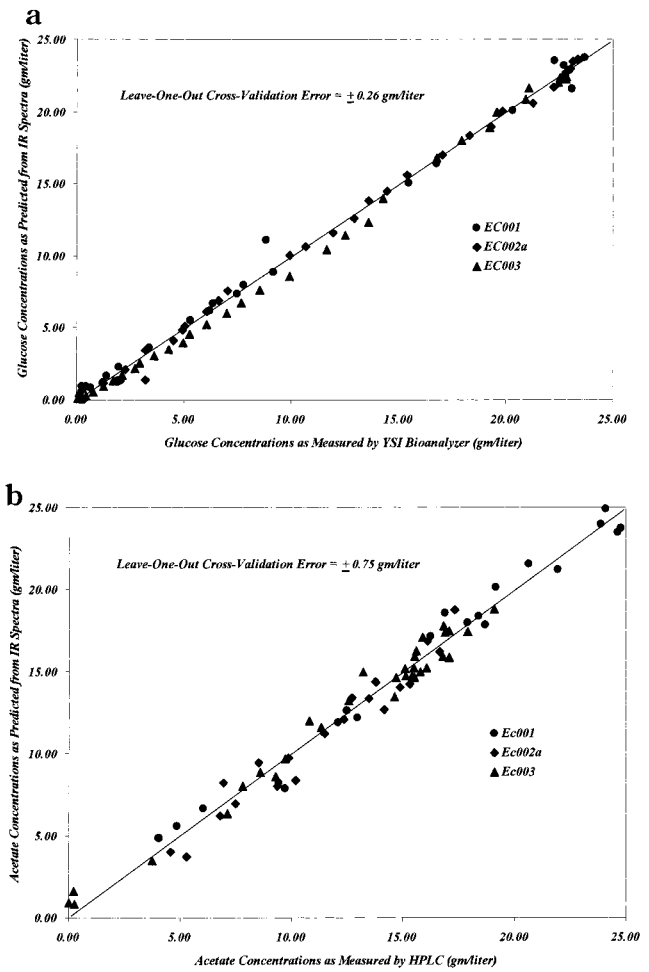

Figure 13. Comparison of measured and predicted concentrations: (a) glucose, (b) acetic acid.

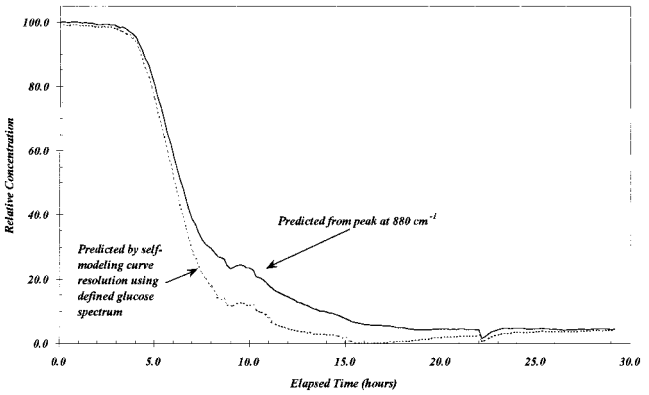

Figure 14. Profile of unknown during fermentation EC001. Relative concentrations were calculated either from profile of absorbance at 880 cm^{-1} or from self-modeling curve resolution of 1225−960 cm^{-1} region.

to detect and qualitatively profile key species not otherwise discernible or easily measured off- or on-line.

The calibration models for glucose and acetic acid constructed from in-process samples covered a wide concentration range and were limited in their accuracy of prediction only by the error inherent in the refereed method used for off-line analysis. Better estimates of the true prediction errors may be obtained by correcting for the errors in the reference methods (Faber and Kowalski, 1997). All models were developed using PLS with no intermediate mathematical manipulation of the spectra, as is typical of the analyses applied to near-IR spectra.

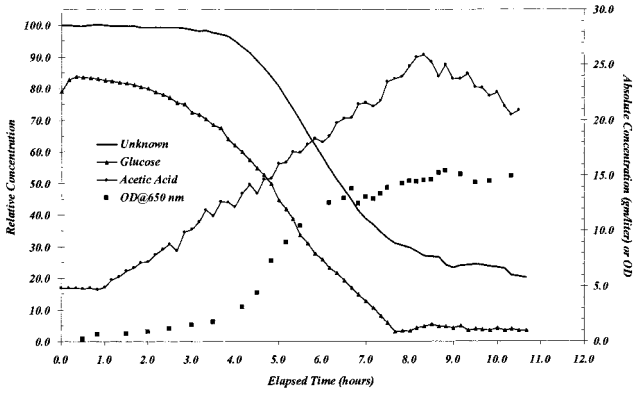

Figure 15. Comparison of relative unknown concentration profile with glucose, acetic acid, and OD profiles for fermentation EC001.

In constructing the calibration/prediction models, all data not identified by the Studentized *t* deleted residual analysis as outliers were used. These data sets are relatively large and, while all the data elements may be sufficient, they may not be necessary for obtaining a robust calibration/prediction model. In addition, on the basis of additional data, it has been determined that the rms prediction errors of the calibration models are most significantly affected by the source of the complex components of the medium. Therefore, it is anticipated that any change in either the source or lot of the medium component would affect the calibration and need to be incorporated for accurate predictions. Both of these issues raise the question of selection of the appropriate calibration data for construction of a prediction model that will account for all influential factors as they are encountered. Obviously, one approach is to incorporate all new process data as it evolves. This approach, however, results in an increasingly large calibration data set. Thus, some future effort needs to be directed toward identifying the minimum size of the calibration set that accounts for all influential factors and produces a robust prediction model. Immediate future work is focused on defining this more rigorous approach to design of the calibration/prediction models, verification of the models' predictive capability through independent experiments, and their use in the closed-loop feedback control of nutrient to the fermentor.

Acknowledgment

The authors express their sincere thanks to ASI Applied Systems for the use of the ReactIR1000/DiComp system and the continual technical support of both the hardware and software that they have provided. We specifically acknowledge the help and encouragement of Don Sting, Henry J. Dubina, Alan J. Rein, Steven M. Donahue, Scott Strand, Norm Van Order, Terry Sauer, and Mark D. Miles. We are also deeply appreciative of the financial support provided through the DuPont Educational Aid Program and the interaction that we have had with Ray Zolandz and Christian Hassel. Finally, we thank SmithKline Beecham for the access to the host *E. coli* strain used in these studies.

References and Notes

(1) Alberti, J. C.; Phillips, J. A.; Fink, D. J.; Wacasz, F. M. Off-Line Monitoring of Fermentation Samples by FTIR/ATR: A Feasibility Study for Real-Time Process Control. *Biotechnol. Bioeng. Symp.* **1985**, No. 15, 689−722.

(2) Bellon-Mauriel, V.; Vallat, C.; Goffinet, D. Quantitative Analysis of Individual Sugars during Starch Hydrolysis by FTIR/ATR Spectrometry. Part I: Multivariate Calibration Study − Repeatibility and Reproducibility. *Appl. Spectrosc.* **1995**, *49* (5), 556−568.

(3) Brimmer, P. J.; Hall, J. W. Determination of Nutrient Levels in a Bioprocess Using Near-Infrared Spectroscopy. *Can. J. Appl. Spectrosc.* **1993**, *38* (6). 155−162.

(4) Cavinato, A. G.; Mayes, D. M.; Ge, Z.; Callis, J. B. Noninvasive Method for Monitoring Ethanol in Fermentation Processes Using Fiber-Optic Near-Infrared Spectroscopy. *Anal. Chem.* **1990**, *62*, 1977−1982.

(5) Chung, H.; Arnold, M. A. Monitoring the Acid-Catalyzed Hydrolysis of Starch with Near-Infrared Spectroscopy. *Appl. Spectrosc.* **1995**, *49* (8), 1097−1102.

(6) Chung, H.; Arnold, M. A.; Rhiel, M.; Murhammer, D. W. Simultaneous Measurements of Glucose and Glutamine in Aqueous Solutions by Near Infrared Spectroscopy. *Appl. Biochem. Biotechnol.* **1995**, *50*, 109−125.

(7) Chung, H.; Arnold, M. A.; Rhiel, M.; Murhammer, D. W. Simultaneous Measurements of Glucose, Glutamine, Ammonia, Lactate, and Glutamate in Aqueous Solutions by Near-Infrared Spectroscopy. *Appl. Spectrosc.* **1996**, *50* (2), 270−276.

(8) Colthup, N. B.; Daly, L. H.; Wiberley, S. E. *Introduction to Infrared and Raman Spectroscopy*; Academic Press: New York, 1990.

(9) Cooper, J. B.; Wise, K. L.; Welch, W. T.; Sumner, M. B.; Wilt, B. K.; Bledsoe, R. R. Comparison of Near-IR, Raman, and Mid-IR Spectroscopies for the Determination of BTEX in Petroleum Fuels. *Appl. Spectrosc.* **1997**, *51* (11), 1613−1620.

(10) Doyle, W. M. Near-IR and Mid-IR Process Analysis—A Critical Comparison. *Technical Note AN-911*; Axiom Analytical Inc.: Irvine, CA, 1995.

(11) Doyle, W. M.; Jennings, N. A. Fourier Transform-Infrared Chemical Reaction Monitoring Using An In situ Deep Immersion Probe. *Spectroscopy* **1990**, *5* (1), 34−38.

(12) Faber, K.; Kowlaski, B. R. Improved Prediction Error Estimates for Multivariate Calibration by Correcting for the Measurement Error in the Reference Values. *Appl. Spectrosc.* **1997**, *51* (5), 660−665.

(13) Fairbrother, P.; George, W. O.; Williams, J. M. Fermentation of Cheese Whey—Monitoring by FT-IR. *Anal. Proc.* **1989**, *26*, 264−267.

(14) Fairbrother, P.; George, W. O.; Williams, J. M. Whey Fermentation: On-Line Analysis of Lactose and Lactic Acid by FTIR Spectroscopy. *Appl. Microbiol. Biotechnol.* **1991**, *35*, 301−305.

(15) Fayolle, P.; Picque, D.; Perret, B.; Latrille, E.; Corrieu, G. Determination of Major Compounds of Alcoholic Fermentation by Middle-Infrared Spectroscopy: Study of Temperature Effects and Calibration Methods. *Appl. Spectrosc.* **1996**, *50* (10), 1325−1330.

(16) Griffiths, P. R.; de Haseth, J. A. *Fourier Transform Infrared Spectroscopy*; John Wiley & Sons: New York, 1986.

(17) Hall, J. W.; McNeil, B.; Rollins, M. J.; Draper, I.; Thompson, B. G.; Macaloney, G. Near-Infrared Spectroscopic Determination of Acetate, Ammonium, Biomass, and Glycerol in an Industrial *Escherichia coli* Fermentation. *Appl. Spectrosc.* **1996**, *50* (1), 102−108.

(18) Hamilton, J. C.; Gemperline, P. J. Mixture Analysis Using Factor Analysis. II: Self-Modeling Curve Resolution. *J. Chemometrics* **1990**, *4* (1), 1−13.

(19) Hammond, S. V.; Brookes, I. K. Near Infrared Spectroscopy—A Powerful Technique for At−Line and On-Line Analysis of Fermentations. In *Harnessing Biotechnology for the 21st Century: Proceedings of the Ninth International Symposium and Exhibition*; Bose, A., Ed.; American Chemical Society: Washington, DC, 1992; pp 325−333.

(20) Harrick, N. J. *Internal Reflection Spectroscopy*; Harrick Scientific Corp.: Ossining, NY, 1979.

(21) Hazen, K. H.; Arnold, M. A.; Small, G. W. Temperature-Insensitive Near-Infrared Spectroscopic Measurement of Glucose in Aqueous Solutions. *Appl. Spectrosc.* **1994**, *48* (4), 477−483.

(22) He, M.; Lorr, D.; Wang, N. S. Microbial Fermentation Monitoring Using Near-Infrared Spectroscopy. *Am. Biotech. Lab.* **1993**, *11*, 56−57.

(23) Hopkinson, J. H.; Moustou, C.; Reynolds, N.; Newbery, J. E. Applications of Attentuated Total Reflection in the Infrared Analysis of Carbohydrates and Biological Whole Cell Samples in Aqueous Solution. *Analyst* **1987**, *112*, 501−505.

(24) Hutson, T. B.; Mitchell, M. L.; Keller, J. T.; Long, D. J.; Chang, M. J. W. A Technique for Monitoring Mammalian Cell Growth and Inhibition in Situ via Fourier Transform Infrared Spectroscopy. *Anal. Biochem.* **1988**, *174*, 415−422.

(25) Kasprow, R. P.; Lange, A. J.; Kirwan, D. J. Correlation of Fermentation Yield with Yeast Extract Composition as Characterized by Near-Infrared Spectroscopy. *Biotechnol. Prog.* **1998**, *14*, 318−325.

(26) Kuehl, D.; Crocombe, R. The Quantitative Analysis of a Model Fermentation Broth. *Appl. Spectrosc.* **1984**, *38* (6), 907−909.

(27) Landau, R. N.; Rein, A. J. *R&D* **1993**, *35* (13), 39−40.

(28) Lee, K. A. B.; Chylla, R. W.; Janota, T. E. Determination of Hydroxyl Number in Polymers by Infrared Spectroscopy: Comparison of Near-IR and Mid-IR. *Appl. Spectrosc.* **1993**, *47* (1), 94−97.

(29) Lin-Vien, D.; Colthup, N. B.; Fateley, W. G.; Grasselli, J. G. *The Handbook of Infrared and Raman Characteristic Frequencies of Organic Molecules*; Academic Press: Boston, 1991.

(30) Macaloney, G.; Hall, J. W.; Rollins, M. J.; Draper, I.; Thompson, B. G.; McNeil, B. Monitoring Biomass and Glycerol in an *Escherichia coli* Fermentation Using Near-Infrared Spectroscopy. *Biotechnol. Lett.* **1994**, *8* (4), 281−286.

(31) Macaloney, G.; Draper, I.; Preston, J.; Anderson, K. B.; Rollins, M. J.; Thompson, B. G.; Hall, J. W.; McNeil, B. At−Line Control and Fault Analysis in an Industrial High Cell Density *Escherichia coli* Fermentation, Using NIR Spectroscopy. *Trans. IChemE.* **1996**, *74*, 212−220.

(32) Mark, H.; Workman, J. *Statistics in Spectroscopy*; Academic Press: Boston, 1991.

(33) Martens, H.; Naes, T. *Multivariate Calibration*. John Wiley & Sons: Chichester, U.K., 1989.

(34) Milosevic, M.; Sting, D., Rein, A. Diamond-Composite Sensor for ATR Spectroscopy. *Spectroscopy* **1995**, *10* (4), 44−49.

(35) Nishinari, K.; Cho, R. K.; Iwamoto, M. Near Infra-Red Monitoring of Enzymatic Hydrolysis of Starch. *Starch/Stärke* **1989**, *41* (3), 110−112.

(36) Peter, D. G.; Hayes, J. M.; Hieftje, G. M. *Chemical Separations and Measurements: Theory and Practice of Analytical Chemistry*; W. B. Saunders Co.: Philadelphia, PA, 1974.

(37) Riley, M. R.; Rhiel, M.; Zhou, X.; Arnold, M. A.; Murhammer, D. W. Simultaneous Measurement of Glucose and Glutamine in Insect Cell Culture Media by Near Infrared Spectroscopy. *Biotechnol. Bioeng.* **1997**, *55* (1), 11−15.

(38) Robinson, J. W. *Undergraduate Instrumental Analysis*; Marcel Dekker: New York, 1995.

(39) Silman, R. W.; Black, L. T.; Norris, K. Assay of Solid-Substrate Fermentation by Means of Reflectance Infrared Analysis. *Biotechnol. Bioeng.* **1983**, *25*, 603−607.

(40) Smith, A. L. *Applied Infrared Spectroscopy—Fundamentals, Techniques, and Analytical Problem-Solving*; John Wiley & Sons: New York, 1979.

(41) Smith, B. C. *Fundamentals of Fourier Transform Infrared Spectroscopy*; CRC Press: Boca Raton, FL, 1996.

(42) Sowa, S.; Towill, L. E. Infrared Spectroscopy of Plant Cell Cultures. *Plant Physiol.* **1991**, *95*, 610−615.

(43) Stallard, B. R. Near-IR Versus Mid-IR: Separability of Three Classes of Organic Compounds. *Appl. Spectrosc.* **1997**, *51* (5), 625−630.

(44) Strobel, H. A.; Heineman, W. R. *Chemical Instrumentation: A Systematic Approach*; John Wiley & Sons: New York, 1989.

(45) Tseng, D. Y.; Vir, R.; Traina, S. J.; Chalmers, J. J. A Fourier Transform Infrared Spectroscopic Analysis of Organic Matter Degradation in a Bench-Scale Solid Substrate Fermentation (Composting) System. *Biotechnol. Bioeng.* **1996**, *52*, 661−671.
(46) Vaccari, G.; Dosi, E.; Campi, A. L.; Gonzalez-Vara yR., A.; Matteuzzi, D.; Mantovani, G. A Near-Infrared Spectroscopy Technique for the Control of Fermentation Processes: An Application to Lactic Acid. Fermentation. *Biotechnol. Bioeng.* **1994**, *43*, 913−917.
(47) White, R. L.; Roberts, D. E.; Attridge, M. C. Fourier Transform Infrared Detection of Pyruvic Acid Assimilation by *E. coli*. *Anal. Chem*. **1985**, *57*, 2487−2491.
(48) Wong, J. S.; Rein, A. J.; Wilks, D.; Wilks, P., Jr. Infrared Spectroscopy of Aqueous Antibiotic Solutions. *Appl. Spectrosc.* **1984**, *38* (1), 32−35.
(49) Yu, K.; Phillips, J. A. The Use of Infrared Spectroscopic Techniques in Monitoring and Controlling Bioreactors. In *Modeling and Control of Biotechnical Processes*; Karim, M. N., Stephanopoulos, G., Eds.; Pergamon Press: Oxford, U.K., 1992; pp 7−14.

Accepted March 19, 1999.

BP990039B